

## Two-Photon Resonant Third-Harmonic Generation in $\text{La}_2\text{CuO}_4$

A. Schülzgen,<sup>1</sup> Y. Kawabe,<sup>2</sup> E. Hanamura,<sup>2</sup> A. Yamanaka,<sup>2</sup> P.-A. Blanche,<sup>1</sup> J. Lee,<sup>1</sup> H. Sato,<sup>3</sup> M. Naito,<sup>3</sup> N. T. Dan,<sup>4</sup>  
S. Uchida,<sup>5</sup> Y. Tanabe,<sup>5</sup> and N. Peyghambarian<sup>1,4</sup>

<sup>1</sup>*Optical Sciences Center, University of Arizona, Tucson, Arizona 85721*

<sup>2</sup>*Chitose Institute of Science and Technology, 758-65 Bibi, Chitose-shi, Hokkaido 066-8655, Japan*

<sup>3</sup>*NTT Basic Research Laboratory, 3-1 Morinosato, Atsugi-shi 243-0198, Japan*

<sup>4</sup>*Cooperative Excitation Project ERATO, Japan Science and Technology Corporation (JST),  
K. S. P. Building D 8th, 3-2-1 Sakato, Takatsu-ku, Kanagawa 213-0012, Japan*

<sup>5</sup>*Department of Applied Physics, University of Tokyo, 7-3-1 Hongo, Bunkyo-ku, Tokyo, Japan*  
(Received 8 June 2000)

Combining linear absorption and nonlinear third harmonic generation (THG) experiments, we investigate details of the electronic structure of the highly correlated electronic system in  $\text{La}_2\text{CuO}_4$ . We demonstrate strong THG mainly due to the charge transfer excitation from O ( $2p_\sigma$ ) to Cu ( $3d_{x^2-y^2}$ ). The THG spectrum shows pronounced features due to three-photon and two-photon resonance enhancement as well as quantum interference effects. We obtain excellent agreement with a THG spectrum calculated in terms of the excitonic cluster model and can identify both odd and even symmetry excitation modes.

DOI: 10.1103/PhysRevLett.86.3164

PACS numbers: 78.47.+p, 42.65.Ky, 74.25.Jb, 74.72.Dn

Recently, there has been considerable interest in highly correlated electronic systems. A prominent example for such a system is  $\text{La}_2\text{CuO}_4$  which is also a parent crystal of high temperature superconductors [1]. It is an antiferromagnetic insulator at and below room temperature. This arises from the strong correlation of  $3d$  electrons and the large overlap between Cu ( $3d_{x^2-y^2}$ ) and O ( $2p_\sigma$ ) orbitals [2]. These characteristics of the perovskite-type structure also result in large oscillator strength of the charge transfer (CT) excitations occurring in the visible region. Not only transport phenomena such as high- $T_c$  superconductivity, but also the optical response can be described by the two-dimensional  $\text{CuO}_2$  network.

Knowledge of the electronic structure of  $\text{La}_2\text{CuO}_4$  is critical to the understanding of highly correlated electronic systems. Spectroscopic methods are among the most powerful tools to gain information which in turn enables the development of proper models for the electronic structures of copper oxides. The linear absorption spectrum of  $\text{La}_2\text{CuO}_4$  shows broadband structures above a CT gap of about 2 eV [3,4]. Although the structure of the absorption spectrum can be qualitatively explained by an excitonic cluster model [5], information is limited because only CT excitations with odd  $E_u$  representation of  $D_{4h}$  symmetry contribute to this spectrum, and broadening effects smear out the spectral features. Even symmetry CT excitation modes, which are expected to be close to the CT gap, are much more difficult to observe in conventional optical experiments since they are not dipole allowed. Large-shift Raman scattering, where the incident photon energy is much larger than the energy of the CT excitations, is one possible technique to find these modes and look at their symmetry properties [6]. Indeed, it has been found that one of the CT excitation modes is located at  $14\,000\text{ cm}^{-1}$  (1.74 eV), just below the CT gap [7]. However, intense

photoluminescence prevents the Raman measurement for higher energy modes.

Nonlinear optical spectroscopy such as third-harmonic generation (THG) should provide key information to solve the above problem. This crystal has inversion symmetry both above and below Néel temperature so that second-harmonic generation is forbidden and THG is the lowest-order nonlinear optical response. The THG process is expected to be enhanced by not only three-photon resonance with dipole-allowed modes but also by two-photon resonance with dipole-forbidden modes. This type of resonance enhancement was already observed in polysilane [8].

In this Letter we show strong THG in thin films of  $\text{La}_2\text{CuO}_4$  that is enhanced by two-photon and three-photon resonant excitation of even and odd symmetry CT modes, respectively. In contrast to the linear absorption, the THG spectrum consists of sharp structures even at room temperature that are provoked by quantum interference effects between different modes of CT excitations in  $\text{La}_2\text{CuO}_4$ . Taking the linear absorption into account, the THG features are clearly assigned in excellent agreement with respect to both odd and even symmetry CT modes obtained by our excitonic cluster model. Our results emphasize the advantages gained by combining nonlinear THG spectroscopy with conventional linear absorption measurements.

THG experiments were performed at room temperature on 180 nm thin films of undoped  $\text{La}_2\text{CuO}_4$  in a typical setup, where the fundamental beam hits the sample through a transparent substrate under normal incidence and the third-harmonic signal is detected from the sample side. The films were grown on  $\text{LaSrAlO}_4$  substrates by molecular beam epitaxy and annealed in a reducing atmosphere to realize the oxygen stoichiometry [9]. Our single crystal films are of excellent optical quality and the orientation of the crystals has been determined by x-ray diffraction.

The  $c$  axis of the crystal is perpendicular to the film plane. For THG measurements, tunable 130 fs pulses are generated by an amplified Ti:sapphire laser system that pumps an optical parametric amplifier at 1 kHz repetition rate. The fundamental photon energy  $\hbar\omega$  is varied between 0.62 and 1.07 eV (5000–8630  $\text{cm}^{-1}$ ). After passing through a spectrometer, the third-harmonic signal in the 1.86–3.21 eV (15 000–25 900  $\text{cm}^{-1}$ ) range is detected by a cooled CCD camera. The third-harmonic signal is then spectrally integrated and the data are carefully corrected for spectral sensitivity of the detection system and reabsorption effects due to linear absorption at the third-harmonic wavelength. Using a thin film of only 180 nm provides the advantage that we do not have to worry about phase matching during the THG process. As a result THG efficiencies can be directly compared over the whole spectral range. THG in the substrate on its own is several orders of magnitude smaller and can be neglected.

Figure 1(a) illustrates the linear absorption spectrum of our sample, while Fig. 1(b) shows the measured third-harmonic intensity as a function of fundamental photon

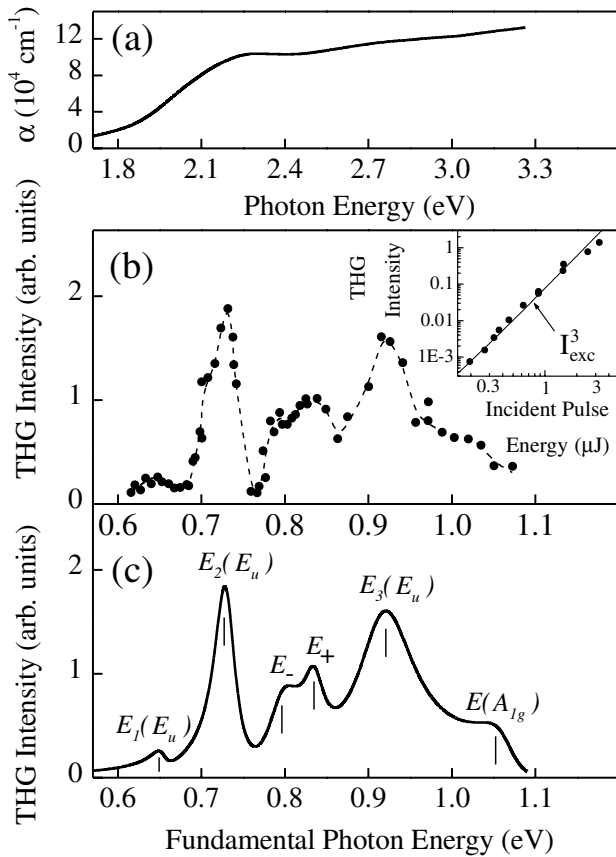


FIG. 1. (a) Absorption spectrum of single crystal  $\text{La}_2\text{CuO}_4$  ( $E \parallel a$ ). (b) Third harmonic intensity vs fundamental photon energy at  $0.3 \text{ J/cm}^2$  incident flux. The dashed line is to guide the eye. Inset: intensity dependence of the third-harmonic signal generated at 2.16 eV on the incident pulse energy at 0.72 eV. The straight line corresponds to a cubic power dependence. (c) Calculated THG spectrum using Eq. (5) with an assignment of the modes responsible for resonant THG enhancement.

energy. Special care has been taken to provide a constant pulse energy of  $3 \mu\text{J}$  for the incident pulses over the whole tuning range that corresponds to an excitation flux of about  $0.3 \text{ J/cm}^2$  after focusing to  $10^{-5} \text{ cm}^2$ . The variation of incident pulse energies over the whole spectral range is within  $\pm 10\%$ . The inset of Fig. 1(b) shows how the generated third-harmonic intensity depends on the incident pulse energy at the pronounced peak for a fundamental photon energy of 0.72 eV. We clearly observe a cubic power dependence of the THG signal on the incident pulse energy over several decades. The energy conversion efficiency is measured to be about  $10^{-4}$  for  $3 \mu\text{J}$  incident pulse energy, resulting in a strong third-harmonic signal, clearly visible with the naked eye, and an excellent signal-to-noise ratio for detection. Note the contrast between the sharp structures in the THG spectrum and the broad features in linear absorption. Within the investigated spectral range the THG signal exhibits a series of pronounced features at 0.65, 0.72, 0.79, 0.84, 0.92, and about 1 eV. Within the experimental error of less than  $\pm 5\%$  no difference in the THG for light polarized parallel to the  $a$  or  $b$  crystal axis is observed. For light polarized at  $45^\circ$  with respect to  $a$  and  $b$  axes the THG signal also does not change for the most part of the spectrum. Only at fundamental energies below 0.75 eV do we observe about 15% decrease in THG intensity.

We compare our data with CT excitation modes calculated by our excitonic cluster model [5]. The optical response is described by a three-band Hubbard Hamiltonian of the two-dimensional  $\text{CuO}_2$  plane: the  $\text{O } 2p_\sigma$  band ( $p_{l\sigma}, p_{l\sigma}^\dagger$ ) with its central energy  $E_p + U_p$  and singly and doubly occupied Cu  $3d_{x^2-y^2}$  bands ( $d_{i\sigma}, d_{i\sigma}^\dagger$ ) with  $E_d$  and  $E_d + U$  as central energies, respectively. This system has the  $D_{4h}$  symmetry and is described by

$$H_{el} = E_d \sum_{i,\sigma} d_{i\sigma}^\dagger d_{i\sigma} + E_p \sum_{l,\sigma} p_{l\sigma}^\dagger p_{l\sigma} + H'_{el} + U \sum_i d_{i\uparrow}^\dagger d_{i\uparrow} d_{i\downarrow}^\dagger d_{i\downarrow} + U_p \sum_l p_{l\uparrow}^\dagger p_{l\uparrow} p_{l\downarrow}^\dagger p_{l\downarrow} + V \sum_{i\sigma\sigma'} \sum_{l \in \{i\}} d_{i\sigma}^\dagger d_{i\sigma} p_{l\sigma'}^\dagger p_{l\sigma'}, \quad (1)$$

$$H'_{el} = t_0 \sum_{i\sigma} \sum_{l \in \{i\}} d_{i\sigma}^\dagger p_{l\sigma} + t_p \sum_{l\sigma} \sum_{l' \in \{l\}} p_{l\sigma}^\dagger p_{l'\sigma}. \quad (2)$$

$U$  and  $U_p$  are the on-site Coulomb repulsions at the Cu and O sites, respectively, and  $V$  is the nearest neighbor Cu-O interatomic Coulomb repulsion. The first and second terms of  $H'_{el}$  in Eq. (2) cause hybridization  $t_0$  between the nearest neighbor Cu and O orbitals and hybridization  $t_p$  between the two nearest neighbor oxygen orbitals, respectively. The electronic ground state  $|g\rangle$  of this Hamiltonian has one electron ( $3d_{x^2-y^2}$ ) per  $\text{Cu}^{2+}$  ion and fully occupied  $2p$  electron states in its surrounding  $\text{O}^{2-}$  ions and is chosen the Néel state in accordance with the experimental observation [5,10,11].

A radiation field can induce CT excitations through the transition dipole moment which is linearly proportional to  $t_0$ . For example, the CT excitation  $\psi^A(1,0) = d_{A1}^\dagger(0,0)p_{it}(1,0)|g\rangle$  represents the formation of a bound CT exciton with the ‘‘electron’’ ( $3d_{x^2-y^2}$ )<sup>2</sup> constituting  $(3d)^{10}$  at the  $A$ -sublattice Cu  $(0,0)$  and the ‘‘hole’’  $(2p)^5$  with spin up at O  $(1,0)$ . Reflecting the  $D_{4h}$  symmetry of the  $\text{CuO}_2$  plane, we obtain four equivalent CT excitations:  $\psi^{A(B)}(1,0)$ ,  $\psi^{A(B)}(0,1)$ ,  $\psi^{A(B)}(-1,0)$ , and  $\psi^{A(B)}(0,-1)$  around the  $A$ -( $B$ -)sublattice Cu ions, corresponding to the four diagrams in Fig. 2(a). Equations (1) and (2) show that the four dipole-allowed states around the  $A$  sublattice are mixed with each other by the second-order process in transfer  $t_0$  between nearest neighbor Cu and O, i.e.,  $t_1 = t_0^2/(U - U_p - E_p - V)$  and by transfer  $t_p$  between nearest neighbor O's. When we diagonalize the energy matrix, we have the eigenfunctions and eigenenergies with the  $A_{1g}$ ,  $B_{1g}$  and the  $E_u^x(E_u^y)$  representation of the  $D_{4h}$  symmetry. The diagonal energy is evaluated to the fourth order in  $t_0$  while the off-diagonal matrix elements of  $H'_{el}$  are calculated to the second order in  $t_0$  and the first order in  $t_p$ . This is a type of degenerate perturbational treatment in  $t_0(t_p)/(U - U_p - E_p)$  or  $t_0(t_p)/(E_p + U_p)$ , and the convergence has been confirmed when we include the cluster size until the fourth nearest neighbor [10]. Only states with odd  $E_u$  symmetry can contribute to absorption and two-magnon Raman scattering [5]. Even symmetry  $A_{1g}$  and  $B_{1g}$  states are observable in two-photon absorption spectra and large-shift Raman scattering.

So far, the optical responses have been analyzed group theoretically by a tetragonal structure  $D_{4h}$  to use the advantage of higher symmetry. However,  $\text{La}_2\text{CuO}_4$  changes to an orthorhombic structure with  $D_{2h}$  symmetry below 511 K [12]. We account for the lower-symmetry crystalline field by perturbational method. The CT excitation of the lowest  $B_{1g}$  state is nearly degenerate with the excitation from  $d_{xy}$  to  $d_{x^2-y^2}$  orbitals within the single Cu ion that has  $A_{2g}$  symmetry in  $D_{4h}$  representation. These two

states merge into  $B_{1g}$  in  $D_{2h}$  representation. Therefore, we make the following linear combinations in  $D_{2h}$  representation, which are hybridized by the lower-symmetry crystalline field  $X$ :

$$\Psi_+ = \cos\theta\Psi(B_{1g}) + \sin\theta\Psi(A_{2g}), \quad (3)$$

$$\Psi_- = -\sin\theta\Psi(B_{1g}) + \cos\theta\Psi(A_{2g}),$$

where  $\tan\theta = X/\{E_+ - E(A_{2g})\}$  and

$$E_\pm = (1/2)\{E(B_{1g}) + E(A_{2g})\} \pm \sqrt{(1/4)\{E(B_{1g}) - E(A_{2g})\}^2 + X^2}.$$

By using the material parameters for the stoichiometric  $\text{La}_2\text{CuO}_4$  crystal with  $D_{4h}$  symmetry ( $E_p = 3$  eV,  $U_p = 3.5$  eV,  $U = 10$  eV,  $V = 0.5$  eV,  $t_0 = 0.82$  eV, and  $t_p = 0.4$  eV), we obtain the odd modes  $E(E_u) = 1.96, 2.12,$  and  $2.80$  eV, and the even modes  $E(B_{1g}) = 1.71$  eV and  $E(A_{1g}) = 2.33$  eV [5,10]. However, the absorption spectrum [Fig. 1(a)] indicates a trace of doped carriers due to weak deviation from the stoichiometry. We also suspect strain induced by the thin film formation [13]. These two effects result in small shifts of transition energies. We choose  $E_1(E_u) = 1.96$  eV,  $E_2(E_u) = 2.19$  eV,  $E_3(E_u) = 2.75$  eV,  $X = 0.04$  eV,  $E(B_{1g}) = 1.635$  eV,  $E(A_{2g}) = 1.625$  eV, and  $E(A_{1g}) = 2.13$  eV. The second  $E_u$  state [ $E_2(E_u)$ ] consists mainly of the dipole-allowed state of Fig. 2(a), while the first and third  $E_u$  states [ $E_1(E_u)$  and  $E_3(E_u)$ ] are hybridized with CT excitations accompanied by two-magnon excitations, as illustrated in Fig. 2(b), as well as unbound electron and hole excitations.

Focusing on THG with nearly two-photon resonant excitation of even symmetry states as intermediate states  $|n\rangle$  and THG with nearly three-photon resonant excitation of  $E_u$  symmetry states as intermediate states, the fourth-order susceptibility tensor which describes THG is expressed as

$$\chi_{\alpha\beta\gamma\delta} = \frac{1}{\epsilon_0} \sum_{\text{even}} \frac{(p_\alpha p_\beta)_{gn}(p_\gamma p_\delta)_{ng}}{\Delta E^2(E_{ng} - 2\hbar\omega - i\Gamma_n)} + \frac{1}{\epsilon_0} \sum_{\text{odd}} \frac{\langle g|p_\alpha|E_u\rangle(p_\beta p_\gamma)_{uu}\langle E_u|p_\delta|g\rangle}{(E_u - 3\hbar\omega - i\Gamma_u)\Delta E'(E_u - \hbar\omega)}. \quad (4)$$

Taking into account the lowest three  $E_u$  modes and three even modes [ $E_-, E_+$ , and  $E(A_{1g})$ ], the THG intensity  $I(3\omega)$ , excluding an unimportant numerical factor, is given by  $|\chi_{\alpha\alpha\alpha\alpha}|^2$  with the same polarization  $\alpha = \beta = \gamma = \delta$  for both incident and THG fields,

$$I(3\omega) = \left| \frac{a_1[A_{1g}]}{E(A_{1g}) - 2\hbar\omega - i\Gamma(A_{1g})} + \frac{\cos\theta a_1[B_{1g}]}{E_+ - 2\hbar\omega - i\Gamma_+} - \frac{\sin\theta a_1[B_{1g}]}{E_- - 2\hbar\omega - i\Gamma_-} - R \sum_j \frac{a_j[E_u]}{E_j(E_u) - 3\hbar\omega - i\Gamma_j} \right|^2. \quad (5)$$

Here  $a_1[A_{1g}]$  and  $a_1[B_{1g}]$  are coefficients of the excited configuration, with  $A_{1g}$  and  $B_{1g}$  representations with the

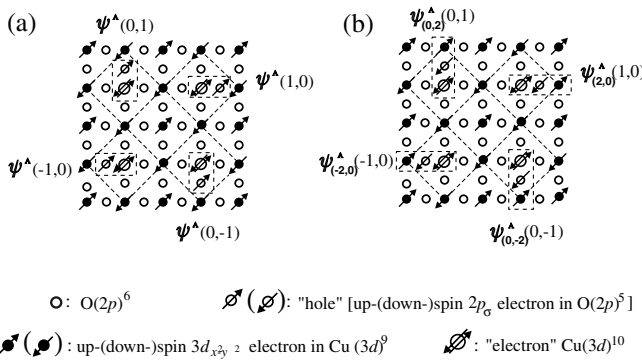


FIG. 2. Diagrams illustrating CT excitations around the  $A$ -sublattice Cu ions in the  $\text{CuO}_2$  plane in  $D_{4h}$  representation (a)  $\psi^A(1,0)$ ,  $\psi^A(0,1)$ ,  $\psi^A(-1,0)$ , and  $\psi^A(0,-1)$  and (b)  $\psi_{(0,2)}^A(1,0)$ ,  $\psi_{(2,0)}^A(1,0)$ ,  $\psi_{(-2,0)}^A(-1,0)$ , and  $\psi_{(0,-2)}^A(0,-1)$  that are CT excitations accompanied by two-magnon excitations.

lowest energies illustrated in Fig. 2(a), while coefficients  $a_j[E_u]$  with the  $j$ th lowest energies are obtained by diagonalizing the CT effects for the dipole-allowed  $E_u$  configurations [5,10]. These values have been obtained in Refs. [10,11] and used to draw Fig. 1(c).

Figure 1(c) shows the THG spectrum for  $\text{La}_2\text{CuO}_4$  calculated using Eq. (5). The relaxation rates  $\Gamma$  were adjusted to achieve the best agreement with the experiment. The relative magnitude  $R$  between two-photon resonant-enhanced THG and three-photon resonant-enhanced THG was chosen to be unity, representing a good approximation of the theoretical value. The excellent agreement with the experiment [Fig. 1(b)] enables us to verify the validity of our model and assign all features present in the experimental THG spectrum. The spectrum is dominated by (i) THG at 0.65, 0.73, and 0.92 eV enhanced by three-photon resonance with  $E_u$  modes at 1.96, 2.19, and 2.75 eV and (ii) THG at 0.79, 0.84, and 1.04 eV enhanced by two-photon resonance with two hybridized  $B_{1g}$  and  $A_{2g}$  modes at 1.59 and 1.67 eV and with an  $A_{1g}$  mode at about 2.13 eV.

Because of the pronounced features observed in the THG spectrum, six eigenenergies of both odd and even symmetry states have been clearly identified and assigned, in contrast to the linear absorption where only dipole-allowed  $E_u$  modes contribute and the spectral features are smeared out. The visibility of the relevant electronic excitations is enhanced by quantum interference between different THG channels that provoke sharp features in the THG spectrum. For example, the distinct dip around  $\hbar\omega = 0.76$  eV is a consequence of destructive interference, mainly between third-harmonic signals enhanced by three-photon resonance of the second lowest  $E_u$  state and by two-photon resonance of the  $E_-$  mode. The appearance of these interference effects emphasizes the advantage of nonlinear spectroscopic techniques such as THG over linear and two-photon absorption spectra, where similar interference effects are absent.

Combining the measured THG spectrum with the theoretical description provides valuable information on the electronic structure in addition to the mode energies. For example, based on the observed polarization dependence, we can exclude a tetragonal structure for  $\text{La}_2\text{CuO}_4$  because, in this case, group-theoretical analysis predicts a large difference in two-photon resonance enhancement be-

tween  $0^\circ$  and  $45^\circ$  polarization relative to the crystalline  $a$  axis [11]. The observations further suggest that twin structures might be induced by the tetragonal-to-orthorhombic structure change and that domains of these twin structures are much smaller than the spot of the laser beam ( $\sim 30 \mu\text{m}$ ).

In conclusion, we have demonstrated strong THG in  $\text{La}_2\text{CuO}_4$  and emphasized the merit of THG experiments for the investigation of energy states and crystal symmetry of insulating transition-metal oxides. Since the THG process is strongly enhanced by both two- and three-photon resonances, we can unambiguously assign even and odd parity modes by comparing one-photon absorption and THG spectra. We find excellent agreement between experimental data and calculations based on the excitonic cluster model, verifying that this model provides an adequate description of the electronic structure in the region of the CT gap. The application of this experimental method to other undoped and doped transition-metal oxides will provide further insight into the electronic structure of these important materials.

- 
- [1] J. G. Bednorz and K. A. Müller, *Z. Phys. B* **64**, 189 (1986).
  - [2] See, for example, M. Imada, A. Fujimori, and Y. Tokura, *Rev. Mod. Phys.* **70**, 1039 (1998), and references therein.
  - [3] Y. Tokura *et al.*, *Phys. Rev. B* **41**, R11 657 (1990).
  - [4] J. P. Falck *et al.*, *Phys. Rev. Lett.* **69**, 1109 (1992).
  - [5] E. Hanamura, N. T. Dan, and Y. Tanabe, *J. Phys. Condens. Matter* **12**, L345 (2000).
  - [6] R. Liu *et al.*, *Phys. Rev. Lett.* **71**, 3709 (1993).
  - [7] D. Salamon *et al.*, *Phys. Rev. B* **51**, 6617 (1995).
  - [8] T. Hasegawa *et al.*, *Phys. Rev. Lett.* **69**, 668 (1992).
  - [9] H. Sato, M. Naito, and H. Yamamoto, *Physica (Amsterdam)* **280C**, 178 (1997).
  - [10] E. Hanamura, N. T. Dan, and Y. Tanabe, *Phys. Rev. B* **62**, 7033 (2000).
  - [11] E. Hanamura, N. T. Dan, and Y. Tanabe, *J. Phys. Condens. Matter* **12**, 8847 (2000).
  - [12] See, for example, B. O. Wells *et al.*, *Science* **277**, 1067 (1997).
  - [13] H. Sato, H. Yamamoto, and M. Naito, *Mater. Res. Soc. Symp. Proc.* **502**, 203 (1998).